The Numerical Solution for a Maxwell Integral Equation: MRI Brain Scan

.

ABSTRACT

This paper uses Maxwell's 4th integral equation model to approximate the magnetic field of an MRI machine given the electric field. MRI scans are a popular method for brain mapping and vital to monitor degenerative diseases of the brain such as Dementia and Alzheimer's. The integral is not analytically solvable, so a numerical approximation is obtained using the Gaussian quadrature method and Romberg's integral method. The approximations are compared in order to obtain good convergence results. The model considers an electrical current and a time dependent electric field. Additionally, understanding the electrical permittivity and conductivity of the brain is critical to tuning the radio frequency of the scan. The assumption is that the MRI scan is of the patient's head.

Keywords: Maxwell integral equation, Gaussian quadrature method, Romberg's integral method, MRI

1. INTRODUCTION

Magnetic resonance imaging, or MRI for short, is a type of procedure doctors use to create images of the body. An MRI scan can produce images of organs, bones, muscles, and blood vessels. To do this, a person is placed within a machine that generates a strong magnetic field. The magnetic field causes atoms to align in the same direction, which are then displaced by radio waves. When the atoms return to their original position, radio signals are released allowing for images to be created (Johns Hopkins Medicine, 2019). This research specifically investigates grey matter as each biological tissue has unique dielectric properties (Abbosh et al., 2024).

* Tel.: 401 254 3097.
E-mail address: ywarnapala@rwu.edu.

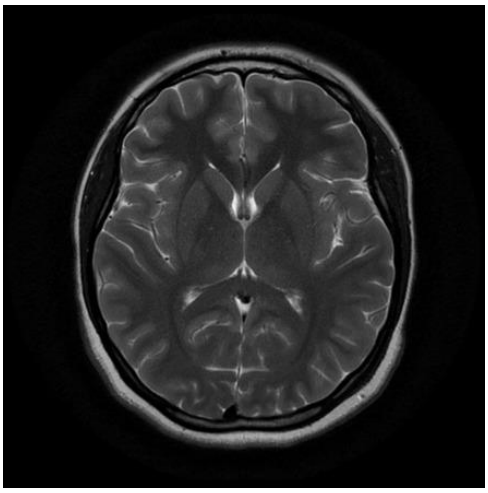

Fig. 1. Image of the human brain from an MRI scan (Radiopaedia, 2024).

1.1 Definitions

We consider the electromagnetic wave propagation in an adult brain with electric permittivity, magnetic permeability, and electrical conductivity. Refer to table 1 for variable details. The electromagnetic wave with frequency is depicted by the following equations:

The Maxwell integral equation is given by

$$\oint_0^L B(l)\, dl = \mu I + \mu\varepsilon \int_0^T \int_0^A \frac{\partial E(a,t)}{\partial t} dadt, \tag{1}$$

where the electrical field is given by (Colton & Kress, 2013)

$$E(a,t) = \left(\varepsilon + \frac{i\sigma}{\omega}\right)^{-\frac{1}{2}} E(a) e^{-i\omega t}, \tag{2}$$

and

$$E(a) = \frac{e^{k|a-t|}}{4\pi|a-t|}. \tag{3}$$

Additionally, the magnetic flux density is given by

$$B(a,t) = \mu^{-\frac{1}{2}} B(a) e^{-i\omega t}. \tag{4}$$

The time dependent Maxwell integral equations follows the following space dependent equations given from (Colton & Kress, 2013)

$$\operatorname{curl} E + \mu \frac{\partial E}{\partial t} = 0, \tag{5}$$

and

$$\operatorname{curl} B - \varepsilon \frac{\partial E}{\partial t} = \sigma E. \tag{6}$$

The space dependent *B* and *E* satisfy the time-harmonic Maxwell equations given by

$$\operatorname{curl} E - ikB = 0, \tag{7}$$

and

$$\operatorname{curl} B - ikE = 0. \tag{8}$$

The wave number k is given by

$$k = ((\varepsilon + \frac{\sigma i}{w})\mu\omega^2)^{1/2}, \tag{9}$$

We chose $\operatorname{Im} k = 0$. Therefore, the mathematical model of the scattering time harmonic waves from an obstacle, a human brain, leads to a boundary value problem for the reduced Maxwell integral equation.

In the following table μ, magnetic permeability, can be considered the absorption coefficient.

Table 1. Units for electric properties

Symbol	Quantity	Units
A	brain surface area	m^2
a	surface area	m^2
B	magnetic flux density	Tesla
I	electrical current (Schmidt & Webb, 2016)	amps
k	electromagnetic wave number	cm^2
l	arc length	m
L	arc length	m
T	time patients are in MRI scan	hr
t	time	hr
ε	relative electrical permittivity (Schmidt & Webb, 2016)	F/m
σ	electrical conductivity (Schmidt & Webb, 2016)	S/m
μ	magnetic permeability	H/m
ω	angular frequency	rad/s

1.2 Theoretical Framework

In (1), the double integral was reduced to a single integral with the assumption that time is bounded. The value of 0.75 hours was used for t. This new integral equation model was given by

$$\oint_0^l B(l)\, dl = \mu I + \mu\varepsilon \int_0^A \frac{\partial E(a,t)}{\partial t} da. \tag{10}$$

Referring to (10), partial derivatives were computed for the real and complex parts of the integrand separately. By taking the partial derivative of (3), we obtained $M = -4\pi k e^{k|a-t|} + \frac{4\pi e^{k|a-t|}}{|a-t|}$, the real portion of the integrand becomes $\int_0^A [\frac{M\cos(\omega t)}{(4\pi|a-t|)^2} - \frac{e^{k|a-t|}}{4\pi|a-t|}\omega sin(\omega t)]\, da$ and the imaginary portion of the integrand becomes $-i\int_0^A [\frac{M\sin(\omega t)}{(4\pi|a-t|)^2} - \frac{e^{k|a-t|}}{4\pi|a-t|}\omega cos(\omega t)]da$.

Together the model is given by

$$\oint_0^L B(l)\,dl = \mu I + \mu\varepsilon\left(\varepsilon + \frac{i\sigma}{\omega}\right)^{-\frac{1}{2}} \int_0^A \left[\frac{M\cos(\omega t)}{(4\pi|a-t|)^2} - \frac{e^{k|a-t|}}{4\pi|a-t|}\omega sin(\omega t)\right] da - i\int_0^A \left[\frac{M\sin(\omega t)}{(4\pi|a-t|)^2} - \frac{e^{k|a-t|}}{4\pi|a-t|}\omega cos(\omega t)\right] da. \quad (11)$$

Refer to table 1.

2. NUMERICAL METHODS

2.1 The Framework of the Gaussian quadrature method

The Gaussian quadrature method was used to modify the integral equation and convert to an integral defined from -1 to 1 defined by the following

$$\int_a^b f(x)\,dx = \int_{-1}^1 f\left(\frac{(b-d)t+(b+d)}{2}\right)\left(\frac{b-d}{2}\right)dt. \quad (12)$$

Using Gaussian Quadrature nodes, the integral was approximated by a numerical sum given by

$$\sum_{i=1}^n c_i P(x_i). \quad (13)$$

where $P(x_i)$ are the Legendre polynomials for n, and c_i are the Gaussian Quadrature weights. We used n = 5 nodes to obtain good convergence results.

If $P(x)$ is any polynomial of degree less than $2n$, then we can convert the integral by a sum given by

$$\int_{-1}^1 P(x)dx = \sum_{i=1}^n c_i P(x_i) \quad (14)$$

where

$$c_i = \int_{-1}^1 \prod_{\substack{j=1 \\ j\neq 1}}^n \frac{x-x_j}{x_i-x_j}\,dx. \quad (15)$$

The method was chosen due to the strategically selected nodes from the Lagrange polynomials. This method allows for good convergence results for ellipsoidal regions.

2.2 The Framework of Romberg's Integration method

To validate our results from the Gaussian Quadrature method, we approximated our integral equation using Romberg's integral method. This method is based on an advanced form of composite trapezoidal rule given by

$$\frac{h}{2}[f(a) + 2\sum_{j=1}^{n-1} f(x_j) + f(b)]. \quad (16)$$

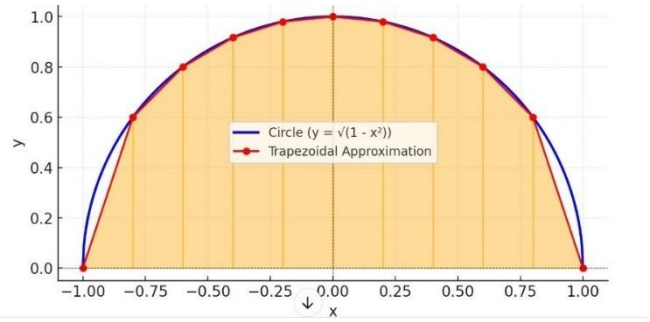

Fig. 2. Sample image of how trapezoidal rule is used to approximate a curve.

Romberg's approximation is given by

$$R_{i,k} = \frac{4^i R_{i-1,k} - R_{i-1,k-1}}{4^i - 1}. \tag{17}$$

$R_{i,k}$ represents the approximation of the integral at the i-th row and k-th column. Romberg's integration is an extrapolation technique which takes a sequence of solutions to an integral and calculates a better approximation.

$$\begin{array}{l} R_{1,1} \\ R_{2,1}\ R_{2,2} \\ R_{3,1}\ R_{3,2}\ R_{3,3} \\ \vdots \quad \vdots \quad \vdots \\ R_{n,1}\ R_{n,2}\ R_{n,3}\ \cdots\ R_{n,n} \end{array}$$

Fig. 3. The Romberg's integral diagram

Romberg's method was chosen in attempt to see how well an advanced form of the trapezoidal method could approximate an ellipsoidal region.

3. NUMERICAL RESULTS

3.1 Gaussian Quadrature Approximations

The following figures show the relationships between each variable and its impact on the magnetic flux density, *B*.

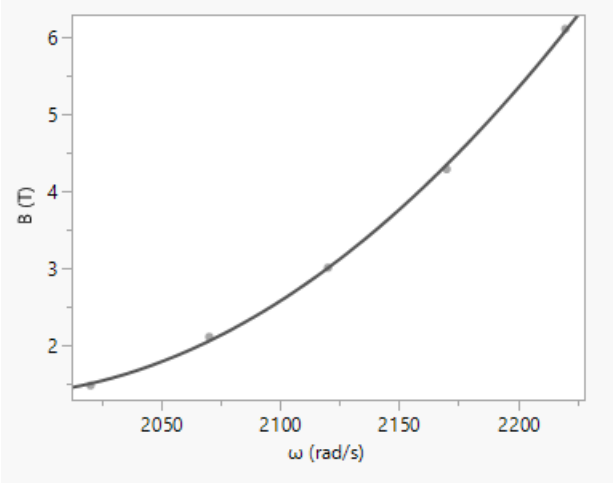

Fig. 4. The effects of variation of angular frequency.

In the above figure, the interval 2020 to 2220 cm^{-1} with the Gaussian Quadrature approximation. The model was given by

$B(\omega) = -45.49231 + 0.0228768\omega + 0.000078823(\omega - 2120)^2$. The rate of change of the magnetic flux density in terms of angular frequency at 2120 rad/s is given by 0.0228768. This is a reasonable rate of change.

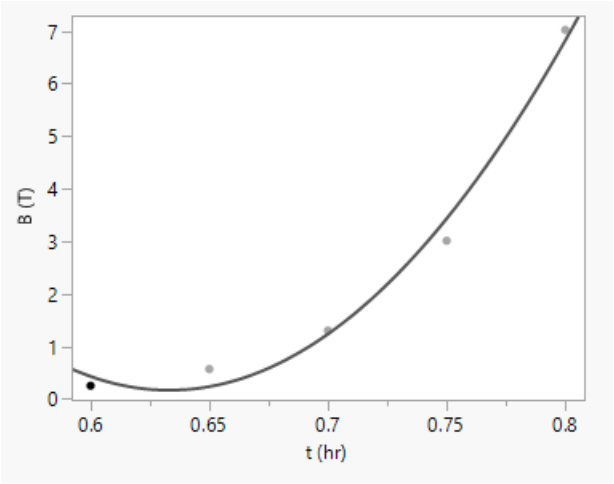

Fig. 5. The effects of variation of time.

In the above figure, the interval 0.6 to .8 hours with the Gaussian Quadrature approximation. The model is given by $B(t) = -21.14066 + 31.96712t + 239.02146(t - 0.7)^2$. The rate of change of the magnetic flux density in terms of time has a rapid change at approximately 39 minutes.

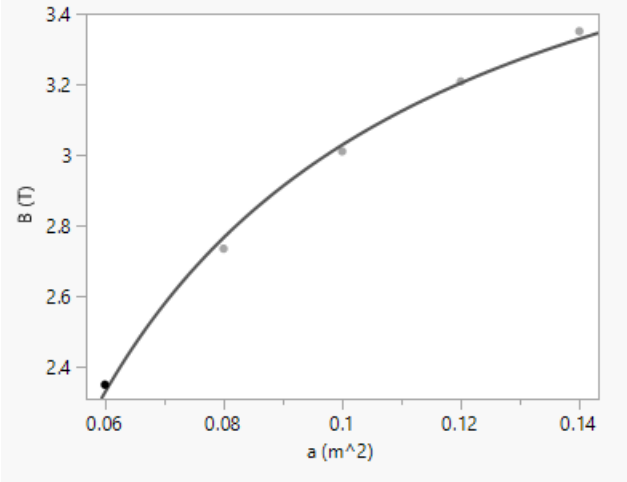

Fig. 6. The effects of variation of area.

In the above figure, the interval 0.06 to .14 meters^2 with the Gaussian Quadrature approximation. The model is given by $B(a) = 4.0789938 - 0.1050665(\frac{1}{a})$. The rate of change of the magnetic flux density in terms of surface area ranges from 7.29628472 to 16.4166406, representing a child brain to an adult brain. This is only considering the change of area, and all other variables are kept constant.

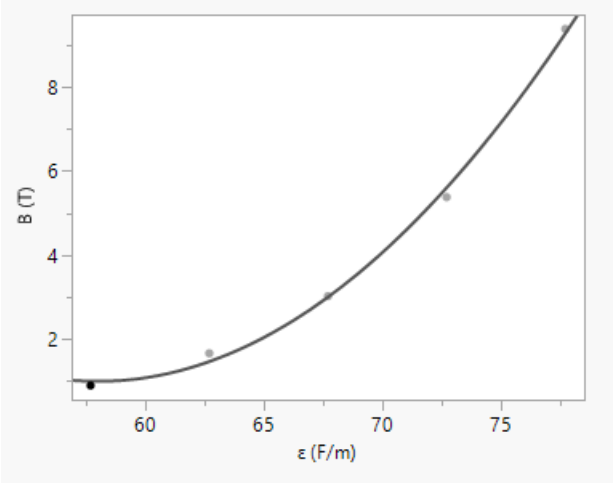

Fig. 7. The effects of variation of relative electrical permittivity.

In the above figure, the interval 57.7 to 77.7 Farads/meter with the Gaussian Quadrature approximation. The model is given by $B(\varepsilon) = -17.19093 + 0.2849845\varepsilon + 0.0144537(\varepsilon - 67.7)^2$. The rate of change of the magnetic flux density in terms of relative electrical permittivity is increasing. Thus, the higher the frequency, the higher the rate of change.

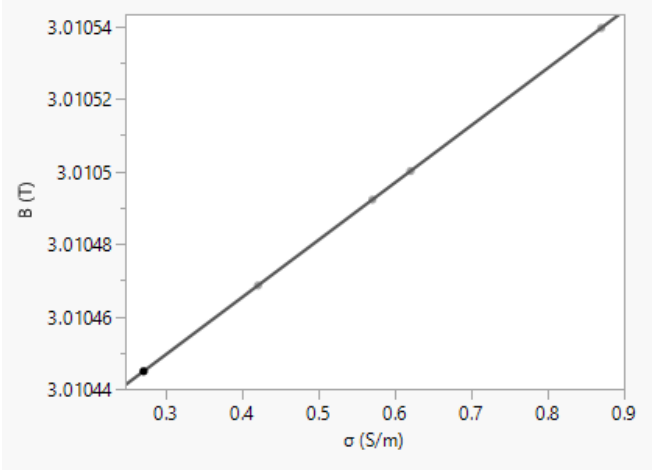

Fig. 8. The effects of variation of electrical conductivity.

In the above figure, the interval 0.27 to 0.87 Siemens/meter with the Gaussian Quadrature approximation. The model is given by $B(\sigma) = 3.0104023 + 0.0001576\sigma$. The rate of change of the magnetic flux density in terms of electrical conductivity is given by 0.0001576. Thus, the magnetic flux density and electrical conductivity are directly proportional.

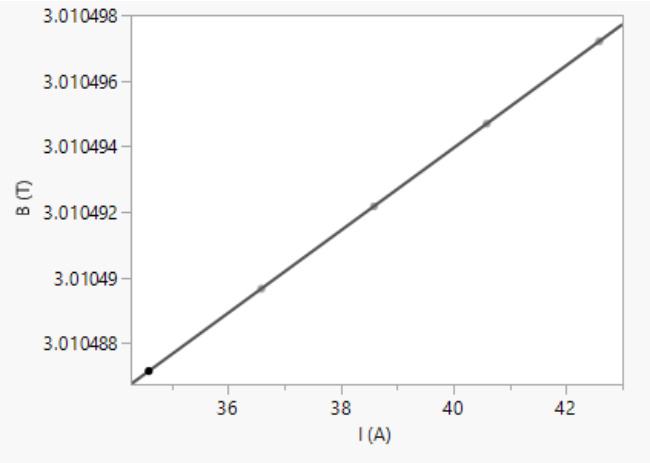

Fig. 9. The effects of variation of electrical current

In the above figure, the interval 34.589 to 42.589 amps with the Gaussian Quadrature approximation. The model is given by $B(I) = 3.0104437 + 0.0000012565I$. The rate of change of the magnetic flux density and electrical current are directly proportional. The higher the current, the higher the magnetic flux density in an MRI brain scan.

3.2 Romberg Approximations

The Romberg figures for angular frequency, surface area, relative electrical permitivity, electrical conductivity, and electrical current were similar to the Gaussian Qudrature figures, except for the magnetic flux density in terms of time, given by figure 3.

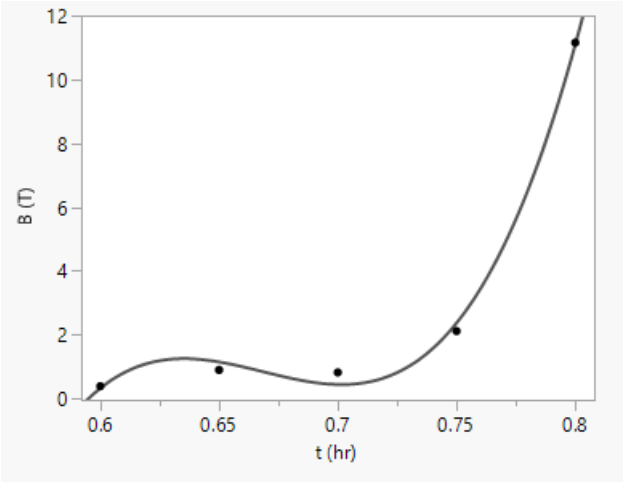

Fig. 10. The effects of variation of time.

In the above figure, the interval 0.6 to .8 hours with the Romberg's approximation. The model is given by $B(t) = 1.6377515 + 1.7068899t + 526.62232(t - 0.7)^2 + 5554.5386(t - 0.7)^3$. Let $\frac{dB}{dt} = P(t)$ and $P'(t)$ is changing from a negative growth rate to a positive growth rate between time of 0.65 and 0.7.

3.3 Approximation Tables

Table 2 to table 7 compares the Gaussian Quadrature approximations to the Romberg approximations. Each highlighted approximation falls within approximately 3 and 7 Tesla. We obtained the following values for the given variables see table 1 where the citations are included.

Table 2. The magnetic flux density versus angular frequency.

ω (rad/s)	Gaussian Quadrature Approximation (n=5)	Romberg Approximation $R_{15,15}$
2020	1.48032196	0.08357981
2070	2.11159406	0.82315871
2120	3.01049217	2.11631864
2170	4.28994208	4.22204993
2220	6.11033835	7.47317820

The variables were $\varepsilon = 67.7\frac{\mathrm{F}}{\mathrm{m}}, \sigma = 0.57\ \frac{\mathrm{S}}{\mathrm{m}}, \mu = 4\pi 10^{-7}\frac{\mathrm{H}}{\mathrm{m}}, I = 38.589\ \mathrm{amps}, t = 0.75\ \mathrm{hr}, \mathrm{and}\ a = 0.1\ \mathrm{m}^2$.

Table 3. The magnetic flux density versus time.

Time (hr)	Gaussian Quadrature Approximation (n=5)	Romberg Approximation $R_{15,15}$
.6	0.25194142	0.38833686
.65	0.56930675	0.89837299
.7	1.30229513	0.82113636
.75	3.01049217	2.11631864
.8	7.02312865	11.15603600

The variables were $\varepsilon = 67.7\frac{\mathrm{F}}{\mathrm{m}}, \sigma = 0.57\ \frac{\mathrm{S}}{\mathrm{m}}, \mu = 4\pi 10^{-7}\frac{\mathrm{H}}{\mathrm{m}}, I = 38.589\ \mathrm{amps},\ \omega = 2120\frac{\mathrm{rad}}{\mathrm{s}}, \mathrm{and}\ a = 0.1\ \mathrm{m}^2$.

Table 4. The magnetic flux density versus time

Area (m^2)	Gaussian Quadrature Approximation (n=5)	Romberg Approximation $R_{15,15}$
0.06	2.34996622	1.89666554
0.08	2.73485727	2.04114519
0.1	3.01049217	2.11631864
0.12	3.20821544	2.15577796
0.14	3.35030169	2.17670071

The variables were $\varepsilon = 67.7\frac{\mathrm{F}}{\mathrm{m}}, \sigma = 0.57\ \frac{\mathrm{S}}{\mathrm{m}}, \mu = 4\pi 10^{-7}\frac{\mathrm{H}}{\mathrm{m}}, I = 38.589\ \mathrm{amps},\ t = 0.75\ \mathrm{hr}, \mathrm{and}\ \omega = 2120\frac{\mathrm{rad}}{\mathrm{s}}$. The best results for adult brains were with an area between 0.1 m^2 and 0.14 m^2.

Table 5. The magnetic flux density versus electrical permittivity.

ε (F/m)	Gaussian Quadrature Approximation (n=5)	Romberg Approximation $R_{15,15}$
57.7	0.87394413	0.63012826
62.7	1.64467706	1.17016128
67.7	3.01049217	2.11631864
72.7	5.37734408	3.73915099
77.7	9.39793994	6.47024540

The variables were $\sigma = 0.57\ \frac{\mathrm{S}}{\mathrm{m}}, \mu = 4\pi 10^{-7}\frac{\mathrm{H}}{\mathrm{m}}, I = 38.589\ \mathrm{amps}, t = 0.75\ \mathrm{hr}, \omega = 2120\frac{\mathrm{rad}}{\mathrm{s}},\ \mathrm{and}\ a = 0.1\ \mathrm{m}^2$. The best approximation, as previously suggested, was 67.7 F/m for electrical permittivity (Schmidt & Webb, 2016).

Table 6. The magnetic flux density versus electrical conductivity.

σ (S/m)	Gaussian Quadrature Approximation (n=5)	Romberg Approximation $R_{15,15}$
.27	3.01044489	2.11628609
.42	3.01046853	2.11630237
.57	3.01049217	2.11631864
.62	3.01050005	2.11632407
.87	3.01053945	2.11635119

The variables were $\varepsilon = 67.7\,\frac{\mathrm{H}}{\mathrm{m}}, \mu = 4\pi 10^{-7}\,\frac{\mathrm{H}}{\mathrm{m}}, I = 38.589\ \mathrm{amps}, t = 0.75\ \mathrm{hr}, \omega = 2120\,\frac{\mathrm{rad}}{\mathrm{s}},$ and $a = 0.1\ \mathrm{m}^2$. There was minimal change to the magnetic flux density when changing electrical conductivity.

Table 7. The magnetic flux density versus electrical current.

I (amps)	Gaussian Quadrature Approximation (n=5)	Romberg Approximation $R_{15,15}$
34.589	3.01048715	2.11631362
36.589	3.01048966	2.11631613
38.589	3.01049217	2.11631864
40.589	3.01049469	2.11632116
42.589	3.01049720	2.11632367

The variables were $\varepsilon = 67.7\,\frac{\mathrm{H}}{\mathrm{m}}, \sigma = 0.57\,\frac{\mathrm{S}}{\mathrm{m}}, \mu = 4\pi 10^{-7}\,\frac{\mathrm{H}}{\mathrm{m}}, t = 0.75\ \mathrm{hr}, \omega = 2120\,\frac{\mathrm{rad}}{\mathrm{s}},$ and $a = 0.1\ \mathrm{m}^2$. There was minimal change to the magnetic flux density when changing the electrical current.

Clearly, the Gaussian Quadrature method is far superior to the Romberg's integral method when solving the Maxwell integral equation for a space such as the human brain. Compared to the Gaussian quadrature method, the Romberg integral method did not properly converge.

4. DISCUSSION

Our method was able to obtain convergence results between 3 and 7 Tesla. The fitted equations allow for interpolation and modifications of the approximations with any value in our selected ranges for each variable. For extrapolation, there is some uncertainty outside of the given bounds. Additionally, the current approximations do not use definitive vacuum permeability. Published literature has not shown a consistent permeability for gray matter, so we are estimating it around the value for free space, $4\pi 10^{-7}\,\frac{\mathrm{H}}{\mathrm{m}}$. Therefore, this analysis is somewhat sensitive to this value. The approximations were found using the Gaussian Quadrature method and Romberg's method. For both methods, the approximations were compared to achieve the best convergence results. For the Gaussian Quadrature method, a convergence of 10^{-8} was achieved with 5 nodes, while Romberg's method did not converge at $R_{15,15}$. The Romberg results vary significantly from the Gaussian Quadrature approximations and can be interpreted as less reliable. The inability to converge comes from the fact that Romberg's method uses a combination of rectangles and trapezoids to achieve the approximation, while the human brain is not a rectangular region.

The current method investigates using an electric field to approximate the magnetic flux density. Future work could be done to get the electric field given the magnetic flux density, and see how multiple variables interact with each other.

5. CONCLUSION

Previous literature mentions an optimal value of 3 Tesla for an MRI brain scan, but other researchers would like an optimal value closer to 7 Tesla (Formica & Silvestri, 2004). The improved magnetic flux density should yield better

images. As shown in table 3 the optimal time a patient should spend in an MRI scan for a brain image is between 45 minutes to 48 minutes.

This research only looked at the gray matter of a healthy adult brain. In the future, further using this method, one might be able to compare the different electrical fields of white matter versus grey matter, which would be significant for detecting early signs of Dementia or Alzheimer's. Research has shown reduced gray matter counts in human brains with Alzheimer's (Thompson et al., 2003). Additionally, the model has the possibility for finding the electric field given the magnetic flux density. When applying the method to other brain tissues for an unhealthy brain, one would need extra Gaussian quadrature nodes to obtain good convergence results, while the Romberg integral method would not be appropriate.

ACKNOWLEDGEMENTS

We would like to thank the Roger Williams University Provost Fund for allowing us to present a preliminary report of this research at the Joint Mathematics Meeting American Mathematical Society poster session in San Francisco, CA, U.S.A and Seattle, WA, U.S.A.).

AUTHORS' CONTRIBUTIONS

Yajni Warnapala designed the theoretical framework of the study. Sam Bielawa performed the numerical calculations for the study and managed the literature searches. Both authors managed the analysis of the study and read and approved the final manuscript.

REFERENCES

Johns Hopkins Medicine. (2019). Magnetic resonance imaging (MRI). Johns Hopkins Medicine. https://www.hopkinsmedicine.org/health/treatment-tests-and-therapies/magnetic-resonance-imaging-mri

Abbosh, A., Ireland, D., Smith, M., Crozier, S., Zhang, Y., & Mudge, S. (2024). Clinical electromagnetic brain scanner. Scientific Reports, 14(1), 5760. https://doi.org/10.1038/s41598-024-55360-7

Radiopaedia. (2024). Normal brain MRI. https://radiopaedia.org/cases/normal-brain-mri-6

Colton, D. L., & Kress, R. (2013). *Inverse acoustic and electromagnetic scattering theory* (3rd ed.). Springer.

Schmidt, R., & Webb, A. (2016). A new approach for electrical properties estimation using a global integral equation and improvements using high permittivity materials. *Journal of Magnetic Resonance, 262*, 8–14. https://doi.org/10.1016/j.jmr.2015.11.002

ChatGPT. (2025). Image generated from a text prompt. OpenAI. https://platform.openai.com/

Formica, D., & Silvestri, S. (2004). Biological effects of exposure to magnetic resonance imaging: An overview. *Biomedical Engineering Online, 3*, 11. https://doi.org/10.1186/1475-925X-3-11

Thompson, P. M., Hayashi, K. M., de Zubicaray, G. I., Janke, A. L., Rose, S. E., Semple, J., et al. (2003). Dynamics of gray matter loss in Alzheimer's disease. *The Journal of Neuroscience, 23*(3), 994–1005. https://doi.org/10.1523/jneurosci.23-03-00994.2003